Separating the impacts of climate change and human activities on actual evapotranspiration in Aksu River Basin ecosystems, Northwest China

Peng Yang, Jun Xia, Chesheng Zhan, Xuejuan Chen, Yunfeng Qiao and Jie Chen

ABSTRACT

Separating the impacts of climate change and human activity on actual evapotranspiration (ET) is important for reducing comprehensive risk and improving the adaptability of water resource systems. In this study, the spatiotemporal distribution of actual ET in the Aksu River Basin, Northwest China, during the period 2000–2015 was evaluated using the Vegetation Interfaces Processes model and Moderate Resolution Imaging Spectroradiometer-Normalized Difference Vegetation Index. The impact of climate change and human activity on actual ET were separated and quantified. The results demonstrated that: (1) the annual pattern of actual ET per pixel exhibited the highest values for arable land (average 362.4 mm/a/pixel), followed by forest land and grassland (average of 159.6 and 142.8 mm/a/pixel, respectively). Significant increasing linear trends ($p < 0.05$) of 3.2 and 1.8 mm/a were detected in the arable land and forest land time series, respectively; (2) precipitation was the most significant of the selected climate factors (precipitation, average temperature, sunshine duration, and wind speed) for all ecosystems. The second most significant was wind speed; (3) human activity caused 89%, 98%, and 80% of the changes in actual ET of forest, grass, and arable land, respectively, while climate change caused 11%, 2%, and 20% of the changes in actual ET, in the Aksu River Basin during 2000–2015.

Key words | actual evapotranspiration, Aksu River Basin, land use cover change, vegetation interfaces processes model, water balance

Peng Yang
Jun Xia (corresponding author)
Chesheng Zhan
Xuejuan Chen
Key Laboratory of Water Cycle & Related Land Surface Processes, Institute of Geographic Sciences and Natural Resources Research,
Chinese Academy of Sciences,
Beijing 100101,
China
E-mail: *xiaj@igsnrr.ac.cn*

Peng Yang
Xuejuan Chen
University of Chinese Academy of Sciences,
Beijing 100049,
China

Jun Xia
Jie Chen
State Key Laboratory of Water Resources & Hydropower Engineering Sciences,
Wuhan University,
Wuhan 430000,
China

Yunfeng Qiao
Key Laboratory of Ecosystem Network Observation and Modeling, Institute of Geographic Sciences and Natural Resources Research,
Chinese Academy of Sciences,
Beijing 100101,
China

INTRODUCTION

Evapotranspiration (ET) is a significant hydrological factor associated with energy balance and water budget that represents water consumption (Liu *et al.* 2016; Chen *et al.* 2017), but is difficult to evaluate at the catchment scale (Liu *et al.* 2016). The accurate assessment of ET plays an important role in effective water resource management (Yeh *et al.* 1998) and in the quantification of water resource carrying capacity (Loucks 2000). Generally, ET estimation at the basin scale is based on land surface hydrologic models combined with weather data (e.g., Wood *et al.* 1992), land-atmosphere models with reanalysis, or remote sensing (e.g., Rodell *et al.* 2004; Mu *et al.* 2007). Although commonly used and well-established models have typically been verified by flux tower ET observations (e.g., Running *et al.* 1999; Xu *et al.* 2006), results often vary across multiple spatiotemporal scales (Liu *et al.* 2016). In this study, the Vegetation Interfaces Processes (VIP) model established by Mo & Liu (2001) and developed by Mo *et al.* (2011) and Mo *et al.*

doi: 10.2166/nh.2018.136

(2015) was applied to estimate actual ET at the pixel scale of remote sensing imagery, with the incorporation of ground surface properties. The model involves multiple modules that simulate energy, water, and carbon exchanges between terrestrial ecosystems and the atmosphere (Mo *et al.* 2014). Furthermore, the model has been widely applied in China, including the Lushi Basin (Mo *et al.* 2004), Xitiao River catchment (Mo & Meng 2011), Northeast China (Mo *et al.* 2014), and North China (Mo *et al.* 2017). These studies demonstrate the broad applicability of the VIP model.

Climate factors and human activity greatly impact ET (Qiu *et al.* 2008; Liu *et al.* 2010; Zhang *et al.* 2011, 2013; Bai *et al.* 2014; Li 2014; Sun *et al.* 2016). Shi *et al.* (2013) concluded that climate change played the greatest role in changes to global ET during 1982–2008. However, Bai *et al.* (2014) found that the contribution of climate change to the ET trend was weak in the arid region of Northwest China, with relatively strong human activity during 1971–2006 (Bai *et al.* 2014). In addition, separating the contribution of climate change from that of human activity (i.e., irrigation, fertilization, grazing, management practices, and land use changes) is difficult (Lobell *et al.* 2011; Wang *et al.* 2016) yet important for understanding the impact of climate change on water consumption, carbon sequestration, and adaptation strategies (Chen *et al.* 2017). Multiple prior studies have explored the separation and quantification of the contributions of climate change and human activity. For example, Qiu *et al.* (2008) evaluated the ET of winter wheat and its response to different irrigation regimes in the North China Plain. Bai *et al.* (2014) determined that an increase in cropland area explained 60.5% of the increased total ET, and management practices accounted for 16.8% of the increased total ET. Chen *et al.* (2017) concluded that climate change and human activity in the North China Plain contributed 0.188 and 0.466 mm/a, respectively, to the actual ET trend of 0.654 mm/a.

The Aksu River is located in the arid northwest region of China, and nearly half of its water originates as glacier and snow melt from the mountains (Li *et al.* 2016). In recent years, hydrological processes in the basin have been severely affected by climate change. Jiang *et al.* (2005) reported that temperature increases had a greater effect on runoff than precipitation in the Aksu River. Xu *et al.* (2011) determined that a close relationship exists between variations in annual runoff and regional climate change. Li *et al.* (2016) reported that the contributions of climate factors and human activity to the runoff in the Aksu River Basin were 94% and 6%, respectively. However, few studies have attempted to separate and quantify the contributions of climate change and human activity to actual ET in the Aksu River Basin, while simultaneously considering land use changes.

The objectives of this study were to (1) evaluate actual ET in the Aksu River Basin via the VIP model and the Moderate Resolution Imaging Spectroradiometer-Normalized Difference Vegetation Index (MODIS-NDVI); (2) estimate the accuracy of actual ET in the basin based on the VIP model; and (3) quantify the contributions of climate change and human activity to actual ET in the Aksu River Basin.

STUDY AREA AND MATERIALS

Study area

The Aksu River Basin is in the northern Tarim River Basin, Northwest China (Li *et al.* 2016) (Figure 1). The Aksu River is one of the largest tributaries of the Tarim River by runoff volume and covers an area of 5.14×10^4 km^2 (Wang *et al.* 2010). The basin experiences a typical temperate continental climate due to the blocking effect of the terrain and a large distance to the ocean. Thus, a low average annual precipitation (64 mm), high average annual potential ET (1,890 mm), and average annual temperature range (9.2–11.5 °C) are observed in the basin (Xu *et al.* 2011). In addition, basin runoff is primarily derived from the Tienshan Mountains and is influenced by the complex climatic conditions and hydrological environment (Xu *et al.* 2011).

Agricultural development in the Aksu River Basin is dominated by oasis irrigation agriculture, for which the irrigation water originates from the river or reservoirs (Huang *et al.* 2015). Tarim irrigation districts are primarily located in the downstream reaches of the Aksu River Basin, where the highest water consumption occurs (Han *et al.* 2015). Moreover, polluted water in the basin is re-routed for irrigation and vegetable production, causing vegetation degradation and salinization of cultivated land (Ji *et al.*

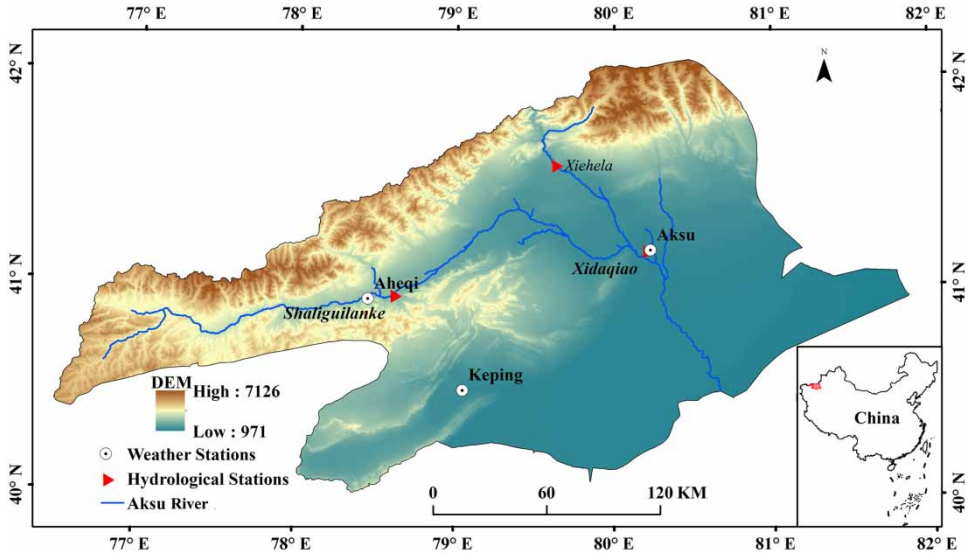

Figure 1 | The study area. (The main image shows the study area, and the inset image shows the location of the study area.).

2000; Guo *et al.* 2003). The difference between the supply and demand for water in the Aksu River Basin is becoming more intense with continued economic development.

Materials

Meteorological data, land use cover change (LUCC) data, digital elevation model data, and MODIS-NDVI were used to drive the VIP model in this study. Meanwhile, hydrometeorological data were applied to construct the water balance (WB) model. Then, a WB-ET model was obtained to verify the results of the VIP model simulation.

Weather and hydrological data

Daily weather data (precipitation (*P*), minimum temperature (T_{mn}), maximum temperature (T_{mx}), relative humidity (*RH*), sunshine duration (*SD*), wind speed (*WS*), and atmospheric pressure (*AP*)) from 2000–2015 at three weather stations were used to drive the VIP model. These data were obtained from the China Meteorological Administration (CMA) (http://data.cma.cn/), as shown in Table 1. The station data were interpolated to the entire basin based on the gradient plus inverse distance squared method proposed by Nalder & Wein (1998). Additionally, runoff data from 2000–2011 were collected from the Annals of Hydrological Statistics, compiled by the Ministry of Water Resources of the People's Republic of China. The monthly averaged runoff was used as hydrological data in this study. The hydrological stations are listed in Table 1.

MODIS-NDVI data

NDVI data for the period of 2000–2015, with a 16-day temporal resolution and 1-km^2 spatial resolution, was downloaded from the MODIS product website (https://lpdaac.usgs.gov/). Missing data at the beginning of 2000 was substituted with that of 2001. NDVI data quality was then improved by application of the Savitzky–Golay (SG) filter (Savitzky & Golay 1964). A smoothing effect was achieved by fitting successive subsets of adjacent data points with a low-order polynomial. The filter can reduce or eliminate the impact of clouds on the quality of remote sensing images. Finally, the 16-day NDVI data was

Table 1 | The summaries of weather and hydrological stations in the Aksu River Basin

Hydrological Stations	Long.(E)	Lat.(N)	Weather Station	Long.(E)	Lat.(N)
Xidaqiao	80.20	41.17	Keping	79.05	40.50
Xiehela	79.61	41.56	Aheqi	78.45	40.93
Shaliguilanke	78.61	40.95	Aksu	80.23	41.17

interpolated to daily data using the Lagrange polynomial method to match the temporal resolution of the VIP model.

LUCC data

(LUCC data for 2000, 2005, and 2010 were provided by the Data Center for Resources and Environmental Sciences, Chinese Academy of Sciences (RESDC) (http://www.resdc.cn). The dataset is primarily based on Landsat Thematic Mapper/Enhanced Thematic Mapper remote sensing images and an artificial visual interpretation method (Liu *et al.* 2014). In this study, 1-km^2 resolution LUCC data were used to drive the VIP model to estimate actual ET during 2000–2002, 2003–2007, and 2008–2015.

METHOD

VIP model

The VIP model simulates canopy transpiration and evaporation from the canopy intercept and soil surface based on the Penman–Monteith equation (Mo *et al.* 2017). Transpiration and photosynthesis processes are coupled by the Ball–Berry relationship between leaf stomatal conductance and net assimilation rate (Mo *et al.* 2017). In terms of the radiation budget, shortwave radiation transfer in the canopy discriminates the near-infrared radiation and leaf spectral properties in the visible range, as well as the proportion of diffusive irradiance and direct beam radiation (Mo *et al.* 2011). The curve-number equation is applied on a daily scale to calculate runoff generation over the land surface using daily net precipitation (Mo *et al.* 2017). The evaporation calculations for soil and vegetation can be expressed as follows:

$$E_c = E_{cp} f_w f_t, \tag{1}$$

$$E_{cp} = \frac{\Delta R_{nc} + f_c \rho_{cp} D / r_a}{(\Delta + \gamma')} \tag{2}$$

where Δ, f_t, and f_w are the slope of the saturation vapor pressure temperature relationship (kPa/°C), the temperature stress factor, and the water stress factor, respectively. Meanwhile, R_{nc}, f_c, ρ_{cp}, D, r_a, and γ' represent net radiation (MJ/m^2/day) absorbed by the canopy, vegetation coverage, specific heat of the air (kJ/kg/°C), saturation vapor pressure (hPa), aerodynamic resistance (kg/m/s^2), and a psychrometric constant considering the least resistance of the leaf (kPa/°C), respectively. Irrigation water is also considered in the VIP model, in which it is assumed that irrigation occurs during some months for some crops, but without considering the specific amount of irrigation. The primary basis is that the soil moisture in arable land after irrigation is regarded as achieving the potential evaporation level. If the potential evaporation is very large and the soil moisture cannot reach the potential evaporation level, the soil water loss is regarded as the actual evaporation. Soil evaporation is limited by the potential evaporation of the surface and the exudation rate of soil moisture. The smaller value is selected as the soil evaporation, as in Equation (3).

$$E_s = \min(E_{sp}, E_{ex}) \tag{3}$$

$$E_{sp} = \frac{\Delta(R_{ns} - G) + (1 - f_c)\rho c_p D / r_a}{\Delta + \gamma'} \tag{4}$$

$$E_{ex} = S\left(t^{0.5} - (t-1)^{0.5}\right) \tag{5}$$

where E_{sp}, E_{ex}, R_{ns}, and G are the potential evaporation of the surface (mm), the leakage rate of soil water (mm), the net radiation absorbed by the soil, and the soil heat flux, respectively. In addition, S is the desorptivity (mm/day$^{0.5}$), generally affected by soil texture, porosity, and other factors; it ranges from 3 mm/day$^{0.5}$ to 5 mm/day$^{0.5}$ (Choudhury & Digirolamo 1998). This study selected an S value of 3 mm/day$^{0.5}$. Meanwhile, f_c is the coverage of surface vegetation, which can be obtained from Equation (6):

$$f_c = 1 - (NDVI_{max} - NDVI / NDVI_{max} - NDVI_{min})^a \tag{6}$$

where $NDVI_{max}$ and $NDVI_{min}$ are the maximum NDVI and minimum NDVI values, respectively. In this formula, a is the empirical value, ranging from 0.6 to 1.25, which was defined as 0.6 in this study.

Water balance model

Similar to the WB model at the catchment scale, the equivalent actual ET in the Aksu River Basin is established

according to:

$$ET = P + (R_{in} - R_{out}) - \Delta S \quad (7)$$

where ET is actual ET (mm), and P (mm), R_{in} (mm), R_{out} (mm), and ΔS (mm) represent precipitation, inflow, outflow, and changes in the terrestrial water storage of the basin, respectively. Because the multiple annually averaged changes in terrestrial water storage can be regarded as zero, Equation (8) can be simplified as:

$$ET = P + (R_{in} - R_{out}) \quad (8)$$

For this study in the Aksu River Basin, two hydrological stations (Shaliguilanke and Xiehela) in the mountainous region were defined as inflow stations, and one station (Xidaqiao) was defined as the outflow station.

Separating the impacts of climate change and human activity

To separate the impacts of climate change and human activity, possible changes in actual ET derived from land use changes were included as impacts of human activity. The difference between the two actual ET trends derived from the two VIP model simulations was attributed to changes in land use, as follows:

$$Q_{LUCC} = T_1 - T_2 \quad (9)$$

where Q_{LUCC} is the change in the trend of actual ET caused by land use change; T_1 is the change in the trend of actual ET derived from the VIP model when considering land use changes (i.e., LUCC data from 2000, 2005, and 2010 were used to drive the VIP model during 2000–2015); and T_2 is the change in the trend of actual ET derived from the VIP model without considering land use changes (i.e., LUCC data from 2000 were applied to drive the VIP model during 2000–2015).

Subsequently, changes in the actual ET caused by other human activities (i.e., irrigation, fertilization, grazing, and management practices, among others) and by climate change are processed based on the methods of Nicholls (1997) and Chen *et al.* (2017). Due to their non-climatic influences on ET (Nicholls 1997; Lobell & Field 2007; Tao *et al.* 2008; Veron *et al.* 2015), these factors can be removed by applying a first-difference detrending method (i.e., the difference of the value between one year and the previous year) (Chen *et al.* 2017). The relationships between the detrended climate factors and the detrended ET are evaluated by partial correlation analysis, which can explore the relationship of two variables independent of the influences of other factors (Nicholls 1997; Xiao *et al.* 2015; Dass *et al.* 2016). The highest partial correlation coefficient indicates the most dominant climate factor (Chen *et al.* 2017).

Multivariate linear regression can quantify the contributions of climate factors (Zhang *et al.* 2010); the major climate factors with detrended processing are the predictor variables for the detrended ET:

$$Y_{ds} = a_1 X_{1ds} + a_2 X_{2ds} + a_3 X_{3ds} + \cdots\cdots \quad (10)$$

where a_i, X_{ids}, and Y_{ds} are the regression coefficients of climate factors, the normalized detrended climate factors, and the normalized detrended actual ET, respectively.

Nicholls (1997) and Lobell & Field (2007) assumed that climate trends and detrended climate factors have similar roles to dependent variables; the contribution of climate factors to the changes in actual ET can be obtained from the regression coefficients and trends of climate factors, as follows:

$$Q_c = \sum_{i=1}^{n} a_i X_{is\_trend} \quad (11)$$

$$Q_{ac} = Q_c / Y_{S\_trend} * \mathrm{Y}_{\mathrm{trend}} \quad (12)$$

where X_{is_trend}, $Q_{c,}$ Y_{s_trend}, Y_{trend}, and Q_{ac} are the trend of normalized climate factors, the climatic contribution to the trend of normalized actual ET, the trend of normalized actual ET, the trend of actual ET, and the actual climatic contribution to the trend of actual ET, respectively.

The remaining trend of actual ET after removing the climatic contribution can be attributed to human activity (i.e., irrigation, fertilization, grazing, and management practices, among others), and can be quantified as follows (Lobell &

Asner 2003):

$$Q_h = Y_{S\_trend} - Q_c \quad (13)$$

$$Q_{ah} = Q_h / Y_{S\_trend} * \mathrm{Y}_{\mathrm{trend}} \quad (14)$$

where Q_h and Q_{ah} are the contribution of human activities to the trend of normalized ET and the actual contribution of human activities to the trend of ET, respectively.

In addition, the relative contributions of climate change and human activity are calculated as:

$$RC_c = |Q_{ac}| / (|Q_{ac}| + |Q_{ah}| + |Q_{LUCC}|) \quad (15)$$

$$RC_h = (|Q_{ah}| + |Q_{LUCC}|) / (|Q_{ac}| + |Q_{ah}| + |Q_{LUCC}|) \quad (16)$$

where RC_c and RC_h are the relative contributions of climate change and human activity, respectively.

RESULTS AND DISCUSSION

LUCC in the Aksu River Basin

Land use changes in the Aksu River Basin were investigated using the LUCC dataset for 2000, 2005, and 2010, as shown in Figure 2. While grassland and glaciers converge in the north of the basin, unused and desert land characterize the southwest of the basin. Grassland covers the largest area of the Aksu River Basin. Arable, residential, and industrial land are mostly located near the middle and lower reaches of the river. Arable land increased from 4,672 km^2 in 2000 to 5,420 km^2 in 2005, and 5,598 km^2 in 2010. In contrast, forest land decreased from 1,291 km^2 in 2000 to 1,213 km^2 in 2005, and 1,203 km^2 in 2010. Similarly, grassland decreased from 19,996 km^2 in 2000, to 19,524 km^2 in 2005, and 19,467 km^2 in 2010. Residential and industrial land collectively increased by 5.6% from 2000 to 2005. Chen *et al.* (2016) observed similar LUCC patterns and reported a decreasing trend in natural land cover and an increase in artificial land cover in the Tarim River Basin.

Because MODIS-NDVI was a significant driving factor of the VIP model, it was also analyzed. The monthly spatiotemporal distribution of NDVI in the Aksu River Basin during 2000–2015 is shown in Figure 3. Figure 3(a) and 3(b) are the original NDVI, while Figure 3(c) and 3(d) are the SG-filtered NDVI. The highest NDVI values were concentrated on the river bank and arable land, and the lowest NDVI was located in the north of

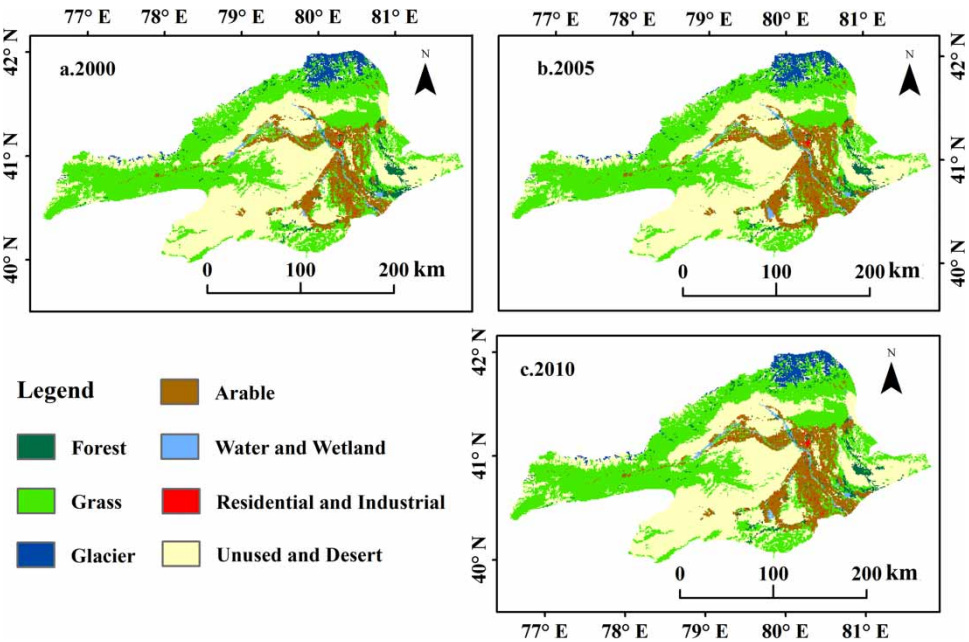

Figure 2 | The land use in the Aksu River Basin during 2000, 2005, and 2010.

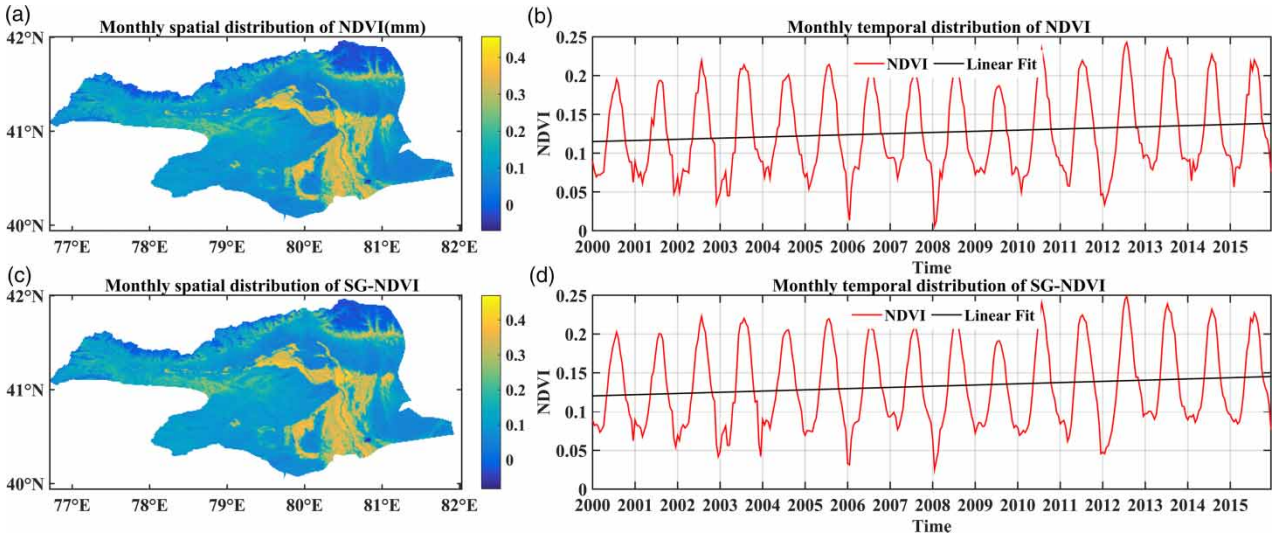

Figure 3 | The spatiotemporal distribution of NDVI in the Aksu River Basin.

the basin in a glaciated area. The NDVI time series exhibited an insignificant increasing trend during 2000–2015, with maximum and minimum NDVI recorded in July 2012 and January 2008, respectively. This increase can be attributed to an increase in arable land during this period (Huang *et al.* 2015). A significant smoothing effect can be seen in Figure 3(d), justifying the use of the filter to eliminate the effect of clouds on the remote sensing images.

Assessment of actual ET using the VIP model

To assess the accuracy of the actual ET derived from the VIP model, the driving factors of the WB model and WB-ET model were analyzed (Figure 4). Precipitation decreased from 2000–2007 but increased from 2008–2011. Meanwhile, the maximum retained runoff (i.e., $R_{in}-R_{out}$) occurred in 2005 and significant seasonal fluctuations are evident in both time series. While the VIP-ET series exhibited

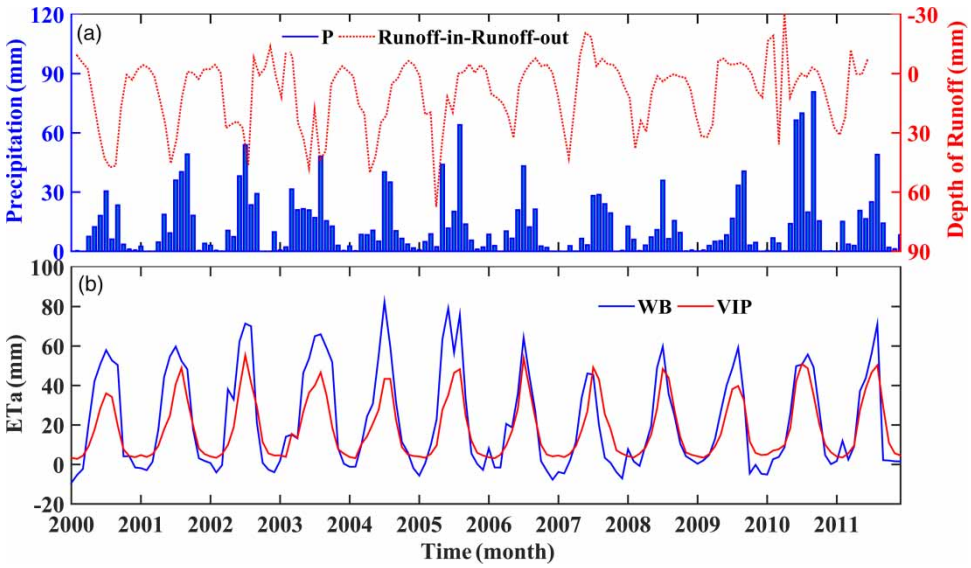

Figure 4 | Comparison of the actual ET for water balance model and VIP model.

significant seasonal fluctuations, VIP-ET displayed a significant correlation with WB-ET. For instance, apart from the period 2003–2005, the amplitudes and phases of the actual ET time series were consistent, with a coefficient of determination of 0.79 at a 95% significance level and a root mean square error (*RMSE*) of 13.7 mm. From this result, we conclude that VIP-ET can be applied to determine the actual ET on the ground, e.g., for vegetation and arable land.

Spatiotemporal distribution of actual ET from the VIP model in the Aksu River Basin

Figure 5 shows the annual spatiotemporal distribution of actual ET derived from the VIP model, including consideration of land use changes. The pixels of actual ET were divided by ecosystem (i.e., forest land, grassland, and arable land) based on LUCC data. The annual mode of actual ET per pixel displays the highest values for arable land (average 362.4 mm/pixel), followed by forest land and grassland (average of 159.6 and 142.8 mm/pixel). In addition, in the annual time series of actual ET (Figure 5(b), 5(d), and 5(f)), the lowest value occurred in 2000 (108 mm for forest, 98 mm for grassland, and 315 mm for arable land), followed by 2009. The highest value occurred in 2013, followed by 2010 and 2003. Significant increasing linear trends ($p < 0.05$) of 3.17 and 1.8 mm/a were observed in arable and forest time series, respectively. As shown in Figure 2, the largest amount of water consumption in grassland can be attributed to this land use type having the largest area. In addition, the increase of actual ET in arable regions was due to the increased arable land area.

To separate the contribution of LUCC to actual ET, the VIP model was run again with climate factors and parameters identical to those used in the first process. However, the input land use was fixed at conditions recorded in 2000. The annual spatial distribution of actual ET from forest, grassland, and arable land is shown in Figure 6(a), 6(c), and 6(e). Arable land displayed the highest per pixel actual ET (367 mm/a/pixel), followed by forest and grassland (162 and 146 mm/a/pixel). In addition, the time series of actual ET (Figure 6(b), 6(d), and 6(f)) displayed significant fluctuations. The grassland and forest land time series exhibited relatively lower actual ET during 2000, 2009, and 2014–2015, while the arable time series was

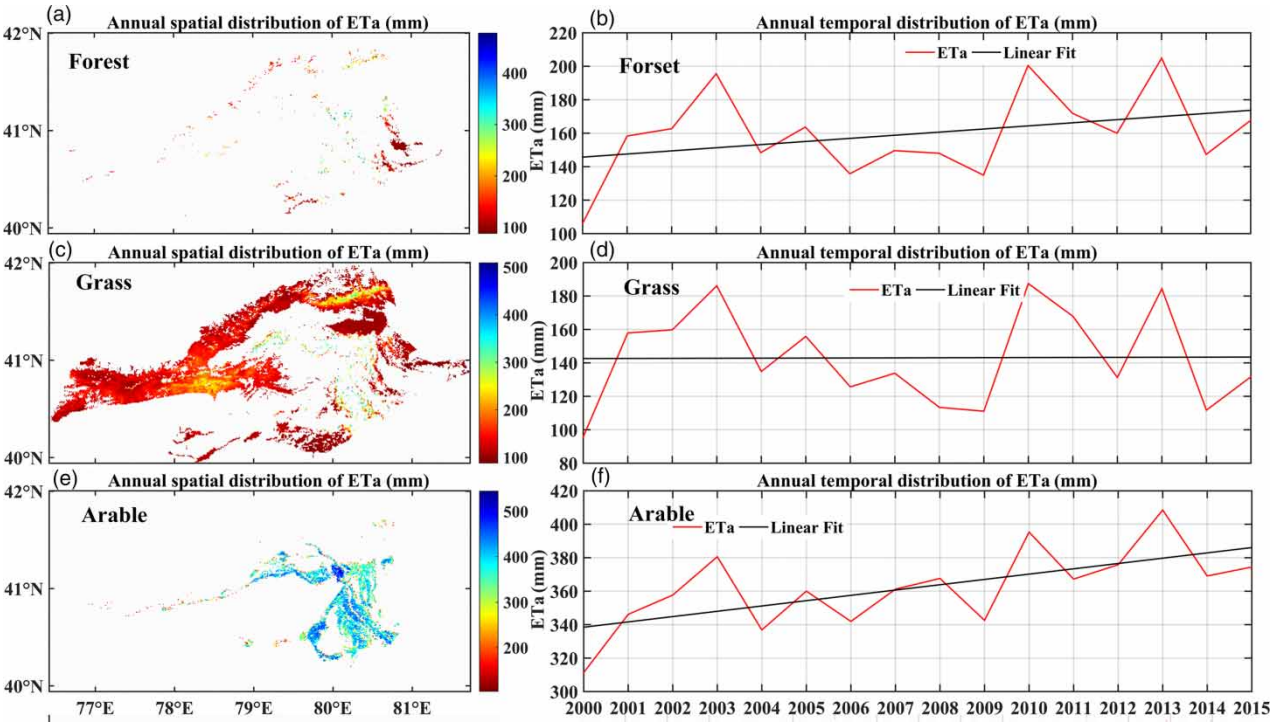

Figure 5 | The spatiotemporal distribution of actual ET in the Aksu River Basin with considering the changes of land use.

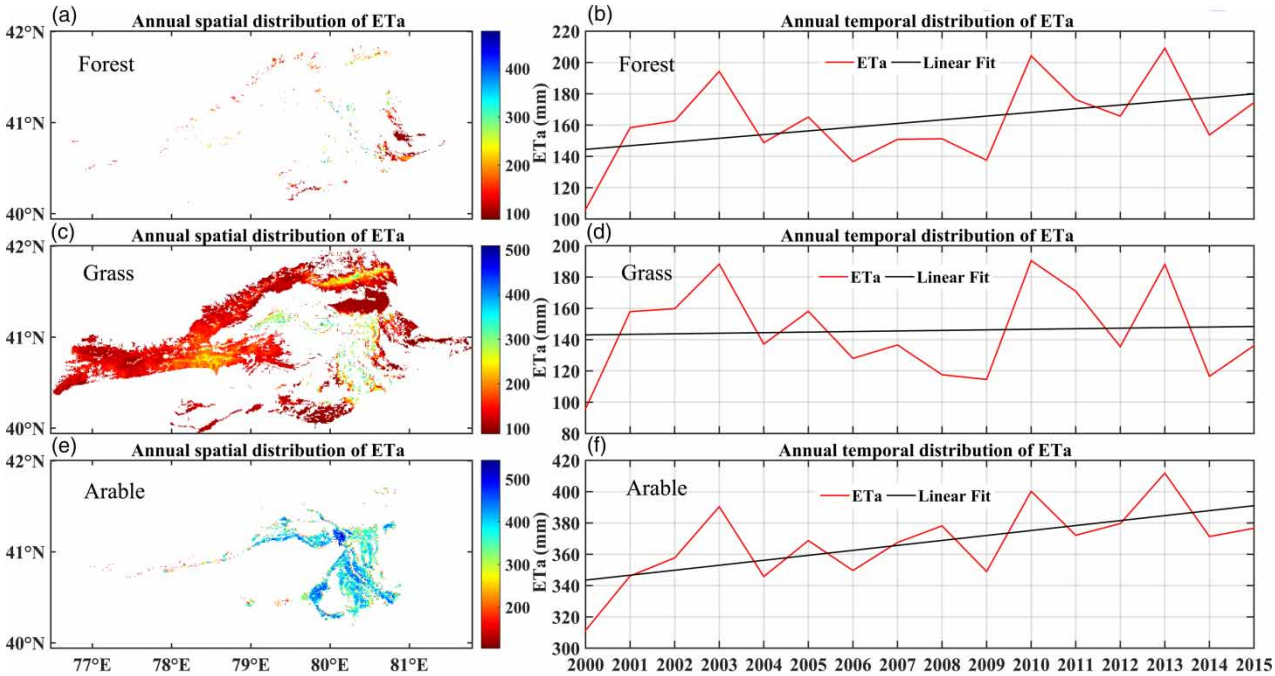

Figure 6 | The spatiotemporal distribution of actual ET in the Aksu River Basin without considering the changes of land use.

more stable. Meanwhile, significant increasing trends ($p < 0.05$) were observed in the time series of actual ET from forest and arable land, which were 2.36 and 3.17 mm/a/a, respectively. Thus, irrespective of land use changes, there was a strong similarity in the spatiotemporal distribution of actual ET derived from the VIP model. The difference in the two slopes for actual ET from the two VIP model runs was regarded as the LUCC contribution. It is notable that there was a difference of 0.5, 0.3, and −0.002 mm/a/a in the results of the VIP model for forest, grass, and arable land cover. This means that LUCC contributed 17.6%, 43.3%, and 0.08% to actual ET for forest, grass, and arable land, respectively.

Separating the impact of climate change and human activity on water consumption in the Aksu River Basin

The VIP model was driven by multiple factors: P, T_a, T_{mx}, T_{mn}, AP, RH, WS, and SD. Thus, the analysis of their impacts on ET is important to quantify the contribution of climate change to actual ET. However, Chen *et al.* (2017) concluded that there were significant auto-correlations among these climate factors. Thus, it was necessary to check the correlation among climate factors prior to multiple regression. The simple correlation coefficients and their significance levels for every two original climate factors and detrended climate factors for forest land, grassland, and arable land are displayed in Figure 7. T_a, T_{mn}, and T_{mx} agree well with each other at the 95% significance level, as does RH with WS and T_a with AP. Ukkola & Prentice (2013) and Cao *et al.* (2014) reported that SD, T_a, P, RH, and WS were the key climate factors influencing ET; thus, T_{mn}, T_{mx}, AP, and RH were not considered in the study. Subsequently, the relationships between ET and the above climate factors (i.e., P, T_a, SD, and WS) were analyzed for the Aksu River Basin.

To obtain the multiple regression models, both the climate factors and actual ET were detrended. Figure 8 depicts the percentile distribution of the original annual actual ET and detrended actual ET for different ecosystems in the Aksu River Basin during 2000–2015. Figure 8(a) shows that the actual ET of arable land is the highest, while Figure 8(b) shows that the detrended actual ET of arable land exhibits the narrowest range. This result means that the impact from climate change on actual ET was evident for arable land, but unclear for grassland. The

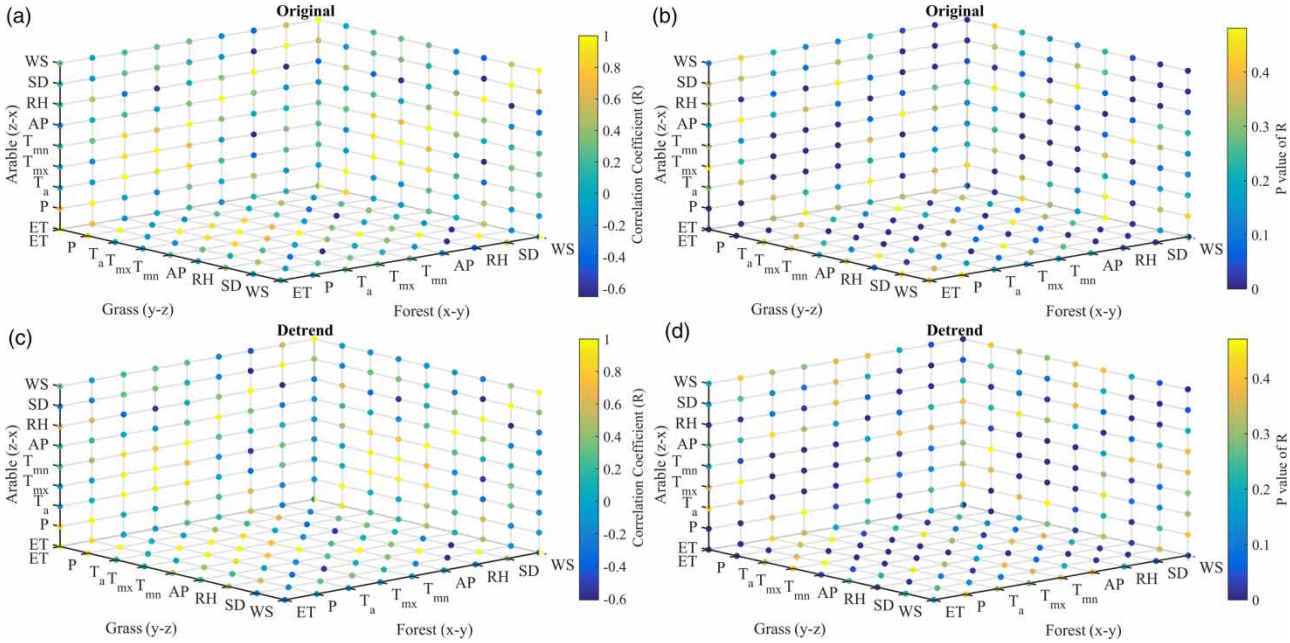

Figure 7 | The correlation coefficients and their significance level for the climate factors driving the VIP model.

normalized regression coefficients for the multiple linear regression model are shown in Table 2. *P* was most significant among the selected climate factors (*P*, T_a, *SD*, and *WS*) for all ecosystems, and *WS* was the second most important. T_a and *SD* displayed varying significance for different ecosystems.

Based on the method of Nicholls (1997) and Chen *et al.* (2017), the contribution of LUCC to actual ET was incorporated into the evaluation. The contributions of climate change and human activity to actual ET in the Aksu River Basin are shown in Table 3. The results indicate that human activity dominated actual ET changes in the Aksu

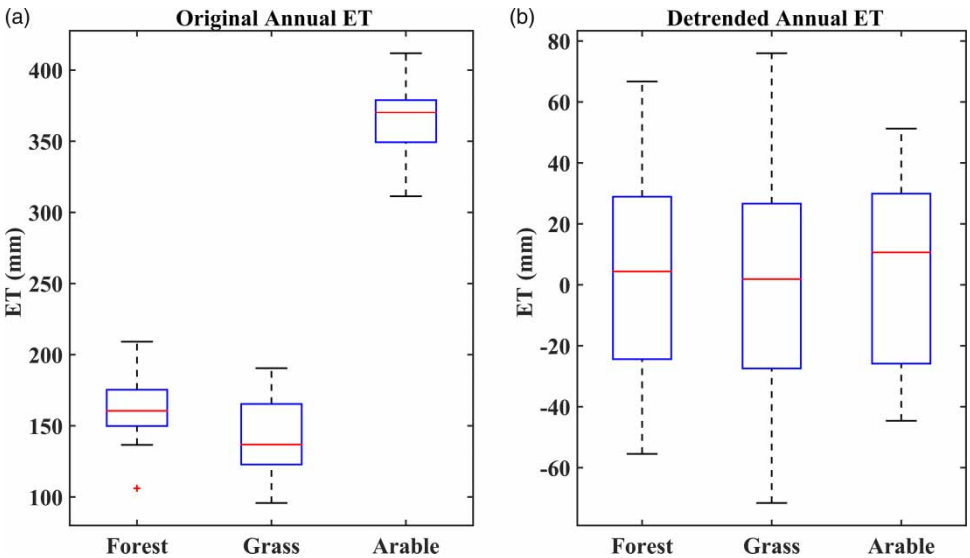

Figure 8 | The ranges of actual ET for the multi-ecosystems in the Aksu River Basin. (The red line represents the median percentile, and the red stars represent the extremes. The whiskers are 5% and 95%). Please refer to the online version of this paper to see this figure in colour: http://dx.doi.org/10.2166/nh.2018.136.

Table 2 | Normalized regression coefficients for the three ecosystems

Categories	a_1	a_2	a_3	a_4
Forest	0.911	0.001	0.068	−0.236
Grass	0.881	0.074	0.148	−0.275
Arable	0.878	−0.19	0.06	−0.222

Table 3 | Contributions of human activities and climate change to actual ET

Categories	Forest	Grass	Arable
Human activities	0.89	0.98	0.80
Climate change	0.11	0.02	0.20

River Basin, while climate change caused less significant changes. Human activity contributed 89%, 98%, and 80% to actual ET changes in forest, grass, and arable land, respectively, and climate change caused actual ET changes of 11%, 2%, and 20%, respectively, during 2000–2015. The relatively well-developed irrigation agriculture and widespread animal husbandry in the basin could result in a more significant impact of human activity on arable land and grassland, but not forest land. Bai *et al.* (2014) determined that this was the case in the Sangonghe Catchment, Northwest China, where human activity explained 77.3% of the changes in actual ET, whereas climate factors accounted for only 22.7%. We conclude that human activity dominates changes in actual ET in the Aksu River Basin.

CONCLUSION

The spatiotemporal distribution of actual ET in the Aksu River Basin during 2000–2015 was evaluated using the VIP model and 1-km^2 MODIS-NDVI data. The actual ET derived from the VIP model was accessed by a WB model, and the contributions of climate change and human activity on the trends of actual ET were separated and quantified. The major conclusions are as follows.

1. Based on LUCC data, a decreasing trend was observed in forest land and grassland, but an increasing trend was observed in arable land in the Aksu River Basin. Arable land increased from 4,672 km^2 in 2000 to 5,420 km^2 in 2005 and 5,598 km^2 in 2010. In contrast, forest land decreased from 1,291 km^2 in 2000 to 1,213 km^2 in 2005 and 1,203 km^2 in 2010. Grassland decreased from 19,996 km^2 in 2000 to 19,524 km^2 in 2005 and 19,467 km^2 in 2010.
2. The annual pattern of actual ET per pixel displayed the highest values for arable land (average 362.4 mm/a/pixel), followed by forest land and grassland (average of 159.6 and 142.8 mm/a/pixel, respectively). Significant increasing linear trends ($p < 0.05$) of 3.2 and 1.8 mm/a were detected in the arable land and forest land time series, respectively. In terms of actual ET derived from the VIP model with constant LUCC, arable land displayed the highest per pixel actual ET (367.2 mm/a/pixel), followed by forest and grassland (162.1 and 145.7 mm/a/pixel, respectively). Meanwhile, significant increasing trends ($p < 0.05$) were observed in the time series of actual ET from forest and arable land, which were 2.4 and 3.2 mm/a, respectively.
3. T_a, T_{mn}, and T_{mx} agreed well with each other at a 95% significance level, as did RH with WS, and T_a with atmospheric pressure. Precipitation was the most important factor affecting the selected climate factors (P, T_a, SD, WS) for all ecosystems, and the second most important factor was wind speed.
4. Human activity contributed 89%, 98%, and 80% to actual ET changes in forest land, grassland, and arable land, respectively, while climate change contributed to actual ET changes of 11%, 2%, and 20%, respectively, in the Aksu River Basin during 2000–2015.

ACKNOWLEDGEMENTS

This research is supported by the National Basic Research Program of China (973 Program, No. 2015CB452701) and the National Natural Science Foundation of China (No. 41571019). The first author thanks the National Aeronautics and Space Administration (NASA) for providing the MODIS data used in this study.

REFERENCES

Bai, J., Chen, X., Li, L., Luo, G. & Yu, Q. 2014 Quantifying the contributions of agricultural oasis expansion, management

practices and climate change to net primary production and evapotranspiration in croplands in arid northwest China. *Journal of Arid Environments* **100**, 31–41.

Cao, G. L., Han, D. M. & Song, X. F. 2014 Evaluating actual evapotranspiration and impacts of groundwater storage change in the North China Plain. *Hydrological Processes* **28** (4), 1797–1808.

Chen, Y. N., Li, Z., Li, W. H., Deng, H. J. & Shen, Y. J. 2016 Water and ecological security: dealing with hydroclimatic challenges at the heart of China's Silk Road. *Environment Earth Science* **75** (10), 881.

Chen, X. J., Mo, X. G., Hu, S. & Liu, S. X. 2017 Contributions of climate change and human activities to ET and GPP trends over North China Plain from 2000 to 2014. *Journal of Geographical Sciences* **27** (6), 661–680.

Choudhury, B. J. & Digirolamo, N. E. 1998 A biophysical process-based estimate of global land surface evaporation using satellite and ancillary data. I. Model description and comparison with observations. *J. Hydrol.* **205** (3–4), 164–185.

Dass, P., Rawlins, M. A., Kimball, J. S. & Kim, Y. 2016 Environmental controls on the increasing GPP of terrestrial vegetation across northern Eurasia. *Biogeosciences* **13** (1), 45–62.

Guo, Y., Xu, H., Li, W. & He, Y. 2003 The investigation on the sewage outlets and the analysis on the water pollution along the mainstream of Tarim River. *Arid Zone Research* **20**, 35–38.

Han, S. M., Hu, Q. L., Yang, Y. H., Wang, J. S., Wang, P. & Wang, Q. 2015 Characteristics and driving factors of drainage water in irrigation districts in arid areas. *Water Resource Management* **29** (14), 5323–5337.

Huang, S., Krysanova, V., Zhai, J. & Su, B. 2015 Impact of intensive irrigation activities on river discharge under agricultural scenarios in the semi-arid Aksu River Basin, Northwest China. *Water Resource Management* **29**, 945–959.

Ji, F., Ma, Y. & Fan, Z. 2000 Salt pollution cycle on cultivated land between drainage and irrigation in the main stream of Tarim River. *Agro-environment Protection* **19**, 133–136.

Jiang, Y., Zhou, C. H. & Cheng, W. M. 2005 Analysis on runoff supply and variation characteristics of Aksu drainage basin. *Journal of Natural Resources* **20** (1), 27–34.

Li, D. 2014 Assessing the impact of interannual variability of precipitation and potential evaporation on evapotranspiration. *Advances in Water Resources* **70**, 1–11.

Li, B. F., Chen, Y. N. & Xiong, H. G. 2016 Quantitatively evaluating the effects of climate factors on runoff change for Aksu River in northwestern China. *Theoretical and Applied Climatology* **123** (1), 97–105.

Liu, Y. A., Wang, E. L., Yang, X. G. & Wang, J. 2010 Contributions of climatic and crop varietal changes to crop production in the North China Plain, since 1980s. *Global Change Biology* **16** (8), 2287–2299.

Liu, J. Y., Kuang, W. H., Zhang, Z. X., Xu, X. L., Qin, Y. W., Ning, J., Zhou, W. C., Zhang, S. W., Li, R. D., Yan, C. Z., Wu, S. X., Shi, X. Z., Jiang, N., Yu, D. S., Pan, X. Z. & Chi, W. F. 2014 Spatio-temporal characteristics, patterns and causes of land-use changes in China since the late 1980s. *Journal of Geographical Sciences* **24** (2), 195–210.

Liu, W. B., Wang, L., Zhou, J., Li, Y. Z., Sun, F. B., Fu, G. B., Li, X. P. & Sang, Y. F. 2016 A worldwide evaluation of basin-scale evapotranspiration estimates against the water balance method. *Journal of Hydrology* **538**, 82–95.

Lobell, D. B. & Asner, G. P. 2003 Climate and management contributions to recent trends in U.S. agricultural yields. *Science* **300** (5625), 1505.

Lobell, D. B. & Field, C. B. 2007 Global scale climate-crop yield relationships and the impacts of recent warming. *Environmental Research Letters* **2** (1), 014002.

Lobell, D. B., Schlenker, W. & Costa-Roberts, J. 2011 Climate trends and global crop production since 1980. *Science* **333** (6042), 616–620.

Loucks, D. P. 2000 Sustainable water resources management. *Water International* **25**, 3–10.

Mo, X. G. & Liu, S. X. 2001 Simulating evapotranspiration and photosynthesis of winter wheat over the growing season. *Agric. For. Meteorol.* **109**, 203–222.

Mo, X. G. & Meng, D. J. 2011 Simulation of the impacts of climate change on the water budget of the Xitiao River catchment, China. *Hyroclimatology: Variability and Change* (S. W. Franks, ed.) **51** (1), 45–65.

Mo, X. G., Liu, S. X., Lin, Z. H. & Zhao, W. 2004 Simulating temporal and spatial variation of evapotranspiration over the Lushi basin. *J. Hydrol.* **285** (1), 125–142.

Mo, X. G., Liu, S. X., Lin, Z. H. & Qiu, J. X. 2011 Patterns of evapotranspiration and GPP and their responses to climate variations over the North China Plain. *Acta Geographical Sinca* **66** (5), 589–598. (in Chinese).

Mo, X. G., Liu, S. X. & Meng, D. J. 2014 Climate variability impacts on evapotranspiration and primary productivity by assimilating remotely sensed data with a process-based model over Songhua River Basin. *International Journal of Climatology* **34**, 1945–1963.

Mo, X. G., Liu, S. X., Lin, Z. H., Wang, S. & Hu, S. 2015 Trends in land surface evapotranspiration across China with remotely sensed NDVI and climatological data for 1981–2010. *Hydrological Sciences Journal-Journal des Sciences Hydrologiques* **60** (12), 2163–2177.

Mo, X. G., Chen, X. J., Hu, S. & Xia, J. 2017 Attributing regional trends of evapotranspiration and gross primary productivity with remote sensing: a case study in the North China Plain. *Hydrology and Earth System Sciences* **21**, 295–310.

Mu, Q., Heinsch, F. A., Zhao, M. & Running, S. W. 2007 Development of a global evapotranspiration algorithm based on MODIS and global meteorology data. *Remote Sensing of Environment* **111** (4), 519–536.

Nalder, I. A. & Wein, R. W. 1998 Spatial interpolation of climatic normals: test of a new method in the Canadian boreal forest. *Agricultural & Forest Meteorology* **92** (4), 211–225.

Nicholls, N. 1997 Increased Australian wheat yield due to recent climate trends. *Nature* **387** (6632), 484–485.

Qiu, G. Y., Wang, L. M., He, X. H., Zhang, X. Y., Chen, S. Y., Chen, J. & Yang, Y. H. 2008 Water use efficiency and evapotranspiration of winter wheat and its response to irrigation regime in the North China Plain. *Agricultural and Forest Meteorology* **148** (11), 1848–1859.

Rodell, M., Famiglietti, J., Chen, J., Seneviratne, S., Viterbo, P., Holl, S. & Wilson, C. 2004 Basin scale estimates of evapotranspiration using GRACE and other observations. *Geophysical Research Letters* **31** (20), 183–213.

Running, S. W., Baldocchi, D. D., Turner, D. P., Gower, S. T., Bakwin, P. S. & Hibbard, K. A. 1999 A global terrestrial monitoring network integrating tower fluxes, flask sampling, ecosystem modeling and EOS satellite data. *Remote Sensing of Environment* **70**, 108–127.

Savitzky, A. & Golay, M. J. E. 1964 Smoothing and differentiation of data by simplified least squares procedures. *Analytical Chemistry* **36**, 1627–1639.

Shi, X. Y., Mao, J. F., Thornton, P. E. & Huang, M. 2013 Spatiotemporal patterns of evapotranspiration in response to multiple environmental factors simulated by the community land model. *Environmental Research Letters* **8** (2), 024012.

Sun, H. Y., Zhang, X. Y., Wang, E. L., Chen, S. Y., Shao, L. W. & Qin, W. L. 2016 Assessing the contribution of weather and management to the annual yield variation of summer maize using APSIM in the North China Plain. *Field Crops Research* **194**, 94–102.

Tao, F. L., Yokozawa, M., Liu, J. Y. & Zhang, Z. 2008 Climate-crop yield relationships at provincial scales in China and the impacts of recent climate trends. *Climate Research* **38** (1), 83–94.

Ukkola, A. M. & Prentice, I. C. 2013 A worldwide analysis of trends in water-balance evapotranspiration. *Hydrology and Earth System Sciences* **17** (10), 4177–4187.

Veron, S. R., de, Abelleyra, D. & Lobell, D. B. 2015 Impacts of precipitation and temperature on crop yields in the pampas. *Climatic Change* **130** (2), 235–245.

Wang, G., Shen, Y., Zhang, J., Wang, S. & Mao, W. 2010 The effects of human activities on oasis climate and hydrologic environment in the Aksu river basin, Xinjiang, China. *Environment Earth Science* **59**, 1759–1769.

Wang, Z., Ye, T., Wang, J., Cheng, Z. & Shi, P. J. 2016 Contribution of climatic and technological factors to crop yield: empirical evidence from late paddy rice in Hunan Province, China. *Stochastic Environmental Research and Risk Assessment* **30** (7), 2019–2030.

Wood, E. F., Lettenmaier, D. P. & Zartarian, V. G. 1992 A land-surface hydrology parameterization with subgrid variability for general circulation models. *Journal of Geophysical Research* **97**, 2717.

Xiao, J. F., Zhou, Y. & Zhang, L. 2015 Contributions of natural and human factors to increases in vegetation productivity in China. *Ecosphere* **6** (11), 1–20.

Xu, C., Gong, L., Jiang, T., Chen, D. & Singh, V. P. 2006 Analysis of spatial distribution and temporal trend of reference evapotranspiration and pan evaporation in Changjiang (Yangtze River) catchment. *Journal of Hydrology* **327**, 81–93.

Xu, J. H., Chen, Y. N., Lu, F., Li, W. H., Zhang, L. J. & Hong, Y. L. 2011 The nonlinear trend of runoff and its response to climate change in the Aksu River, western China. *International Journal of Climatology* **31** (5), 687–695.

Yeh, P. J. F., Irizarry, M. & Eltahir, E. A. B. 1998 Hydroclimatology of Illinois: a comparison of monthly evaporation estimates based on atmospheric water balance and soil water balance. *Journal of Geophysical Research* **103**, 19823.

Zhang, S. H., Liu, S. X., Mo, X. G., Shu, C., Sun, Y. & Zhang, C. 2010 Assessing the impact of climate change on reference evapotranspiration in Aksu River Basin. *Acta Geographical Sinca* **65** (11), 1363–1370. (in Chinese)

Zhang, X. Y., Chen, S. Y., Sun, H. Y., Shao, L. W. & Wang, Y. Z. 2011 Changes in evapotranspiration over irrigated winter wheat and maize in North China Plain over three decades. *Agricultural Water Management* **98** (6), 1097–1104.

Zhang, X. Y., Wang, S. F., Sun, H. Y., Shao, L. W. & Liu, X. W. 2013 Contribution of cultivar, fertilizer and weather to yield variation of winter wheat over three decades: a case study in the North China Plain. *European Journal of Agronomy* **50**, 52–59.

First received 10 August 2017; accepted in revised form 16 June 2018. Available online 6 July 2018